REVISING THE KEPLER-11 SYSTEM: A TESTAMENT TO THE IMPORTANCE OF PRECISE STELLAR CHARACTERIZATION

Megan Bedell[1], Jacob L. Bean[1], Jorge Meléndez[2], Sean Mills[1], Dan Fabrycky[1], Martin Asplund[3], Ivan Ramírez[4], Fan Liu[3], David Yong[3]

Draft version July 25, 2016

ABSTRACT

The six planets of the Kepler-11 system are the archetypal example of a population of surprisingly low-density transiting planets revealed by the *Kepler* mission. We have determined the stellar chemical composition of Kepler-11 to unprecedented precision using an extremely high quality spectrum from Keck-HIRES (R≃67000, SNR≃280). Contrary to previously published results, our spectroscopic constraints indicate that Kepler-11 is a young main-sequence solar twin. The revised stellar parameters raise the densities of the Kepler-11 planets by about 30%, making them more typical of the emerging class of "puffy" close-in exoplanets. We obtain photospheric abundances of 22 elements and find that Kepler-11 is enhanced in refractory materials relative to the solar abundance pattern. We additionally analyze the *Kepler* transits and transit timing variations (TTVs) using a photodynamical model and discuss the tension between spectroscopic and TTV-based stellar density estimates.

Subject headings: stars: abundances, stars: fundamental parameters, techniques: spectroscopic

1. INTRODUCTION

Five years after their initial discovery, the six planets of the Kepler-11 system remain a crown jewel of *Kepler* science results (Lissauer et al. 2011). All six planets orbit a Sun-like host star at low eccentricies in a largely co-planar, tightly packed configuration. The formation and long-term stability of the system remains an open question (see e.g. Ikoma & Hori 2012; Hands et al. 2014; Mahajan & Wu 2014). Kepler-11 is regarded as the prototypical example of a "System with Tightly-Packed Inner Planets" (STIP, Boley et al. 2014, right citation??), a class of *Kepler* multi-planet systems which offer a surprising counterpoint to our own solar system's architecture. Given the low geometric probability of finding a six-planet transiting system, Kepler-11 may be a valuable and rare opportunity to study in detail a common population of exoplanets.

In addition to their unusually tight system architecture, the Kepler-11 planets are noteworthy in another sense: their measured masses and radii place them among the lowest-density super-Earths known to date. Transit timing variations (TTVs) have been measured for all six planets. In the discovery paper, Lissauer et al. (2011) derived mass constraints for the five inner planets based on TTVs from six quarters of *Kepler* data. Migaszewski et al. (2012) reanalyzed the same data using a photodynamical model and found similar results, with an additional constraint on the outermost planet mass. The system was later revisited by Lissauer et al. (2013)

using fourteen quarters of *Kepler* data. All three analyses estimate mean densities of $\leq 0.5\ \rho_\oplus$ for all planets in the system, implying a considerable gas envelope on even the smaller super-Earths. This result has implications for potential formation scenarios, with the viability of forming such low-density planets on short orbits in situ up for debate (e.g. Lopez et al. 2012; Bodenheimer & Lissauer 2014; Howe & Burrows 2015).

Mean planet densities derived from transits and TTVs (or from transits and radial velocities) have a strong dependence on the properties of the host star. Since the transit depth observationally constrains the ratio of planetary radius to stellar radius, the planet volume depends on the assumed stellar radius to the third power. The planet mass found from TTV inversion is correlated with the stellar mass. Host star characterization is therefore a critical part of measuring planet densities.

In past works, Kepler-11 has been characterized only through spectroscopic analysis of low to modest signal-to-noise data. Lissauer et al. (2011, 2013); Rowe et al. (2014) all use spectra taken by Keck with SNR ≤ 40 and apply the Spectroscopy Made Easy package (SME, Valenti & Piskunov 1996) to perform matching to a library of synthetic spectra. The resulting stellar atmospheric parameters, when compared with stellar evolution models, indicate that Kepler-11 is a slightly evolved solar analog with a density of $0.80 \pm 0.04\ \rho_\odot$ (Lissauer et al. 2013). No independent measurements of the stellar density (e.g. from asteroseismology or parallax) are available. Analysis of the stellar composition is also minimal. Adibekyan et al. (2012a) perform an equivalent width (EW) analysis on one of these Keck spectra to derive abundances of three α-elements and find that Kepler-11 has moderately low abundances of Ca, Cr, and Ti; however, the line list employed is quite limited with ≤ 5 lines per element.

Kepler-11's well-characterized planetary system makes it a prime target for more detailed spectroscopic study. In this work, we present an analysis of a new, very high SNR spectrum. We use equivalent widths to measure the

E-mail: mbedell@oddjob.uchicago.edu
[1] Department of Astronomy and Astrophysics, University of Chicago, 5640 S. Ellis Ave, Chicago, IL 60637, USA
[2] Departamento de Astronomia do IAG/USP, Universidade de São Paulo, Rua do Matão 1226, Cidade Universitária, 05508-900 São Paulo, SP, Brazil
[3] Research School of Astronomy and Astrophysics, The Australian National University, Cotter Road, Weston, ACT 2611, Australia
[4] McDonald Observatory and Department of Astronomy, University of Texas at Austin, USA

stellar properties and abundances of 22 elements at high precision.

2. DATA

Owing to its relative faintness (V = 14.2, Lissauer et al. (2011)), Kepler-11 was previously observed only at a signal-to-noise ratio insufficient for high-precision spectroscopic characterization. We dedicated nearly 8 hours of Keck I time to obtaining a higher quality spectrum. Over the course of two consecutive nights (July 26-27 2015), we made 22 1200-s exposures of Kepler-11 for a co-added result of SNR≃280. For these observations, HIRES was used with the B2 slit and kv387 filter, yielding a resolution R≃67000 and wavelength coverage between 390 and 830 nm.

We also observed the Sun (using Ceres) and nine bright potential Kepler-11 twins with the same instrumental setup and similar SNR. The Kepler-11 twins were selected by imposing criteria of $5600 \leq T_{\rm eff} \geq 5750$ K and $4.2 \leq \log g \geq 4.4$ dex on databases of previously published stellar parameters (Adibekyan et al. 2012b; Bensby et al. 2014). Preference was given to stars likely to be thick-disk members with approximately solar metallicity. These criteria were set based on the original spectroscopic analysis of Kepler-11 by Lissauer et al. (2011), who found $T_{\rm eff} = 5680 \pm 100$ K, $\log g = 4.3 \pm 0.2$ dex, [Fe/H]= 0.0 ± 0.1 dex, and a significant chance of Kepler-11's being a thick disk member based on its kinematics.

The spectral extraction was performed by the Mauna Kea Echelle Extraction (MAKEE) pipeline. All Kepler-11 spectra were then co-added using IRAF's *scombine*.[5] Continuum normalization was done by fitting low-order polynomial functions to each order, with care to use the same functional order for a given spectral order on every stellar spectrum to avoid bias in the subsequent differential analysis. Doppler corrections were applied using IRAF's *dopcor* task.

(details about Kepler lightcurve?)

3. STELLAR PROPERTIES FROM SPECTROSCOPIC ANALYSIS

The fundamental properties of Kepler-11 and its potential twins were derived from an equivalent width analysis. We hand-measured 94 Fe I and 17 Fe II spectral lines using IRAF's *splot*. The line list was chosen (criteria, cite). Equivalent widths were measured by carefully choosing local continua as described in Bedell et al. (2014) to maximize differential precision between the spectra. The full line list and measured equivalent widths are available in Table 2.

The stellar effective temperature $T_{\rm eff}$, surface gravity $\log g$, metallicity [Fe/H], and microturbulence v_t were determined by imposing requirements of excitation and ionization balance on the iron abundances derived by MOOG (Sneden 1973). It is important to note that we exclusively used the differential abundance measurements relative to the solar spectrum. By directly comparing line-by-line differential abundances of spectrally similar stars, we minimize the influence of stellar model
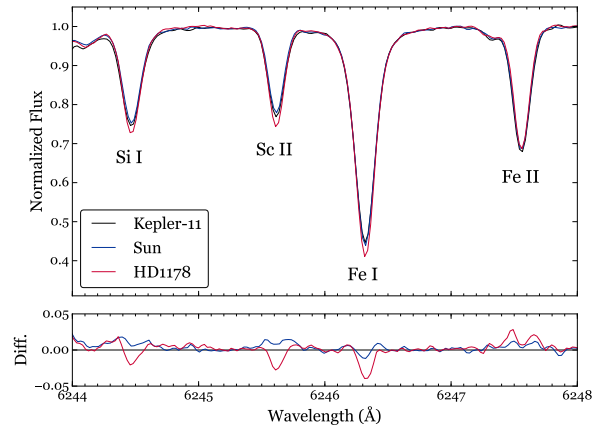
FIG. 1.— A small section of the Keck-HIRES spectra of the Sun (blue), Kepler-11 (black), and HD1178 (red), which has fundamental parameters similar to those given by Lissauer et al. (2013) for Kepler-11. Residuals for flux relative to the Kepler-11 spectrum are plotted in the lower panel.

systematics on the final parameters and abundances (see e.g. Ramírez et al. 2014). Parameter solutions were found iteratively using the q^2 python package.[6] Uncertainties were determined by propagating scatter among the measured line abundances as described in Epstein et al. (2010); Bensby et al. (2014).

The resulting stellar parameters for all observed stars are given in Table 1. The $T_{\rm eff}$ and $\log g$ for Kepler-11 are significantly higher than previously determined values. For example, Lissauer et al. (2013) find $T_{\rm eff} = 5666 \pm 60$ K, $\log g = 4.28 \pm 0.07$ dex, and [Fe/H]= 0.00 ± 0.04 dex, while we find $T_{\rm eff} = 5839 \pm 7$ K, $\log g = 4.45 \pm 0.02$ dex, and [Fe/H]= 0.06 ± 0.01 dex. Potential sources of this tension include the substantially different SNR of spectra used and the difference in analysis technique. Lissauer et al. (2013) and other previous analyses use SME, which employs a library of synthetic spectra to do spectral matching.

Our revised stellar parameters securely place Kepler-11 in the solar twin category. This can be seen even by eye: as depicted in Figure 1, at high SNR Kepler-11's spectrum is nearly identical to the solar spectrum and distinctly different from that of HD1178, the star from our sample whose fundamental parameters most closely match those found by Lissauer et al. (2013). In particular, the solar-like $\log g$ for Kepler-11 implies that it is denser and less evolved than previously thought.

We used stellar evolutionary models to estimate the mass, radius, and age of Kepler-11. Yonsei-Yale isochrones were fit using q^2. We also applied Dartmouth and Basti isochrones using the *isochrones* python package for fitting. All three models gave results consistent within well below 1σ. From these fits, we estimate a stellar mass $M_\star = 1.04 \pm 0.01\ M_\odot$, radius $R_\star = 1.00 \pm 0.02\ R_\odot$, and age 2.8 ± 0.8 Gyr. This gives a stellar density $\rho_\star = 1.47 \pm 0.09$ g cm^{-3}.

4. ALTERNATIVE STELLAR AGE INDICATORS

While mass, radius, and density cannot be measured through other methods from the stellar spectrum, stel-

TABLE 1
SUMMARY OF DERIVED FUNDAMENTAL STELLAR PROPERTIES.

Spectrum	$T_{\rm eff}$ (K)	σ_T (K)	$\log g$ (dex)	σ_{logg} (dex)	v_t (km s^{-1})	σ_{v_t} (km s^{-1})	[Fe/H] (dex)	$\sigma_{[Fe/H]}$ (dex)
Sun (Ceres) [a]	5777	–	4.44	–	0.97	–	0.0	–
K11	5840	7	4.46	0.02	1.00	0.02	0.063	0.007
HD1178	5644	10	4.34	0.03	0.89	0.03	0.013	0.010
HD10145	5627	20	4.33	0.05	0.81	0.06	-0.017	0.021
HD16623	5833	47	4.51	0.09	1.07	0.10	-0.434	0.034
HD20329	5592	16	4.32	0.04	0.80	0.05	-0.094	0.015
HD21727	5608	21	4.32	0.06	0.82	0.07	0.010	0.020
HD21774	5757	27	4.33	0.06	0.99	0.06	0.251	0.024
HD28474	5808	43	4.60	0.08	1.06	0.10	-0.578	0.030
HD176733	5597	15	4.33	0.04	0.77	0.05	-0.012	0.014
HD191069	5739	29	4.33	0.09	1.03	0.08	-0.029	0.025

[a]Used as reference star.

FIG. 2.— Spectra and synthetic fit for Kepler-11 (red) and the Sun (blue) around the Li I 6707.8 Å line.

lar age has multiple known proxies. We used several alternate methods to measure the age of Kepler-11 as an independent test of its evolutionary state. The results unanimously agree upon a sub-solar age for Kepler-11. Details of the methods used follow.

4.1. *Stellar Rotation*

The apparent rotation rate $v \sin i$ was measured using five saturated lines (Fe I 6027.050 Å, 6151.618 Å, 6165.360 Å, 6705.102 Å, and Ni I 6767.772 Å) from the Keck spectrum. The procedure used is described in depth in dos Santos et al. (2016), and will be summarized here. We first measured the macroturbulence value $v_{\rm macro}$ for each line in the solar reference spectrum with MOOG *synth*. We then calculated $v_{\rm macro}$ for Kepler-11 using the measured solar values and the empirical relation given in Equation 1 of dos Santos et al. (2016). Finally, MOOG *synth* was used to find $v \sin i$ for each line in Kepler-11's spectrum with $v_{\rm macro}$ fixed to the calculated value.

The five lines give a consistent result of $v \sin i = 2.2 \pm 0.2$ km s^{-1}. Assuming alignment of the stellar spin axis with the orbital axis of its transiting planets, we can take $v \sin i$ as the true rotational velocity. This translates to an age of **x** using **x**, or **x** from dos Santos et al. (2016)'s updated relation.

4.2. *Lithium Abundance*

The lithium abundance of Kepler-11 was measured by synthesizing the Li I 6707.8 Å line with MOOG *synth*. The line list was adopted from Meléndez et al. (2012) and includes blends of atomic and molecular lines. We find a lithium abundance of $A({\rm Li}) = 1.26 \pm 0.05$, higher than the solar value of 1.11 at the level of 3σ (Figure 2). This implies a sub-solar age.

4.3. *[Y/Mg] Abundance Ratio*

Recent works by Nissen (2015) and Tucci Maia et al. (2016) have identified the ratio of yttrium to magnesium abundances as an excellent proxy for age in main-sequence Sun-like stars. We measured these abundances as described in Section 5 and found a [Y/Mg] ratio of **x**. Using the age relation from Tucci Maia et al. (2016), this suggests an age of 4.0 ± 0.7 Gyr.

4.4. *Chromospheric Emission*

We measured the chromospheric emission level of Kepler-11 using the Ca II H&K lines in the spectrum. finish

5. STELLAR ABUNDANCES

We measured photospheric abundances using the curve-of-growth technique for 20 other elements (excluding lithium, whose synthesis-based abundance determination is discussed in Section 4.2). As with the iron lines, all equivalent widths were measured by hand and line-by-line differential abundances determined with MOOG using q^2. The line list was adapted from (details). Hyperfine structure corrections were applied for Co I, Cu I, Mn I, V I, and Y II following (cite). Carbon abundances were measured by a combination of C I and CH lines. Errors on the final abundances were found by adding in quadrature the intrinsic scatter of the lines and the uncertainty propagated from errors on the stellar parameters, as described in (cite). The measured equivalent widths are given in Table 2, and resulting abundances for all stars are in Table 3.

Kepler-11's status as a solar twin enables direct comparison of its abundance pattern to that of the Sun and other known solar twins. Of particular interest is the question of trends in elemental abundances with condensation temperature (T_C). As shown by Meléndez et al. (2009), the solar abundance pattern is unusual in its depletion of refractory elements relative to volatiles. This depletion has been interpreted as "missing" rocky material that is locked up in the Solar System planets (Chambers 2010). Building up the number of stars with precisely characterized abundance patterns and planetary systems can help to test this possibility.

We apply corrections for the effects of galactic chemical evolution (GCE), which can change the abundance patterns and T_C trends of stars at varying ages (Nissen 2015; Spina et al. 2016b). We correct each abundance [X/H] using the prescription of Spina et al. (2016a), who fit hyperbolic relations to [X/H] as a function of stellar age for a sample of solar twins. We then use the corrected abundances and T_C values from Table 8 of Lodders (2003) to search for a trend. For this part of the analysis, all measured states of a given element (e.g. CI and CH, TiI and TiII, etc.) were combined with a weighted average for the overall elemental abundance.

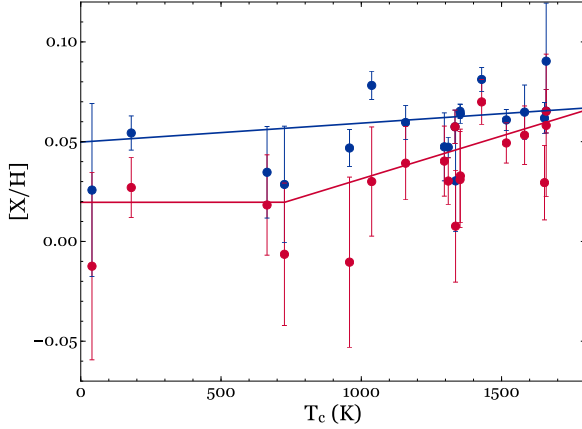Based on our analysis, Kepler-11 appears to be a "typ-

FIG. 3.— Differential element abundances of Kepler-11 as a function of the condensation temperature of the element within the protoplanetary disk. The spectral abundances are plotted in blue, and abundances after a GCE correction is applied are in red. Best-fit models were derived using a

ical" solar twin: that is, its abundance pattern is enhanced in refractories relative to the solar pattern (Figure 3). The significance of this enhancement depends on the stellar age adopted for the GCE correction. Without GCE correction applied, the T_C slope is significant only at the 2σ level, whereas adopting an age of 2.8 Gyr enhances the slope to nearly 5σ. (compare to Melendez2009)

6. STELLAR PROPERTIES FROM TRANSIT & TTV ANALYSIS

write this section

7. DISCUSSION

7.1. *Discrepancies in Stellar Densities*

The stellar densities found through spectroscopic characterization (1.47 ± 0.09 g cm^{-3}) and photodynamical modeling (1.13 ± 0.07 g cm^{-3}) are inconsistent at the level of $\sim 3\sigma$. While spectroscopically-derived densities can be strongly dependent on imperfect stellar isochrone models, we note that in this case Kepler-11's extreme similarity to the Sun places it near the anchor point of most models, increasing the accuracy of isochronal analysis. Moreover, multiple independent methods support the result of a young, non-evolved age and therefore a solar-like density for Kepler-11.

An alternative hypothesis is that some bias in the transit analysis has resulted in an erroneously low inferred stellar density. As described by Kipping (2014), multiple effects can bias the density measured by transits, including stellar activity, blended background sources, and non-zero planet eccentricities. (discuss in detail)

7.2. *Implications for Planets*

The mass and radius of Kepler-11 has considerable repercussions for its planetary system. We approximate the planet mass derived from TTVs as a linear function of the assumed stellar mass. The planet radius also has a linear dependence on stellar radius, since only the relative surface areas of planet and star can be measured by the transit depth. The stellar properties obtained through spectroscopic analysis therefore raise the planet masses by a factor of 8% and lower the planet radii by
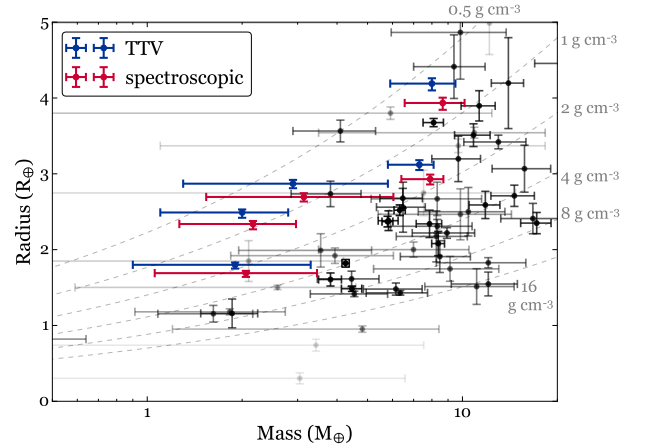

FIG. 4.— Exoplanets with measured masses and radii. Transparencies of the black points scale with the relative error on planet parameters. Kepler-11 a-e are plotted in red (using the transit and TTV-derived parameters) and blue (adjusted by the spectroscopic stellar parameters). Dashed lines show fixed mean densities.

a factor of 6% relative to the transit and TTV-derived values. The results are shown in Figure 4.

Adopting the stellar properties from spectroscopic analysis raises the mean densities of the Kepler-11 planets by $\sim 30\%$. This change may go a long way in resolving... finish

8. CONCLUSION

Using an extremely high-quality spectrum of the multi-planet host star Kepler-11, we have... finish

Facilities: Keck:I (HIRES), Kepler

REFERENCES

Adibekyan, V. Z., Delgado Mena, E., Sousa, S. G., et al. 2012a, A&A, 547, A36
Adibekyan, V. Z., Sousa, S. G., Santos, N. C., et al. 2012b, A&A, 545, A32
Bedell, M., Meléndez, J., Bean, J. L., et al. 2014, ApJ, 795, 23
Bensby, T., Feltzing, S., & Oey, M. S. 2014, A&A, 562, A71
Bodenheimer, P., & Lissauer, J. J. 2014, ApJ, 791, 103
Boley, A. C., Morris, M. A., & Ford, E. B. 2014, ApJ, 792, L27
Chambers, J. E. 2010, ApJ, 724, 92

dos Santos, L. A., Meléndez, J., do Nascimento, Jr., J.-D., et al. 2016, A&A, arXiv:1606.06214
Epstein, C. R., Johnson, J. a., Dong, S., et al. 2010, The Astrophysical Journal, 709, 447
Hands, T. O., Alexander, R. D., & Dehnen, W. 2014, MNRAS, 445, 749
Howe, A. R., & Burrows, A. 2015, ApJ, 808, 150
Ikoma, M., & Hori, Y. 2012, ApJ, 753, 66
Kipping, D. M. 2014, MNRAS, 440, 2164

Lissauer, J. J., Fabrycky, D. C., Ford, E. B., et al. 2011, Nature, 470, 53

Lissauer, J. J., Jontof-Hutter, D., Rowe, J. F., et al. 2013, ApJ, 770, 131

Lodders, K. 2003, ApJ, 591, 1220

Lopez, E. D., Fortney, J. J., & Miller, N. 2012, ApJ, 761, 59

Mahajan, N., & Wu, Y. 2014, ApJ, 795, 32

Meléndez, J., Asplund, M., Gustafsson, B., & Yong, D. 2009, ApJ, 704, L66

Meléndez, J., Bergemann, M., Cohen, J. G., et al. 2012, A&A, 543, A29

Migaszewski, C., Słonina, M., & Goździewski, K. 2012, MNRAS, 427, 770

Nissen, P. E. 2015, A&A, 579, A52

Ramírez, I., Meléndez, J., Bean, J., et al. 2014, A&A, 572, A48

Rowe, J. F., Bryson, S. T., Marcy, G. W., et al. 2014, ApJ, 784, 45

Sneden, C. A. 1973, PhD thesis, THE UNIVERSITY OF TEXAS AT AUSTIN.

Spina, L., Meléndez, J., Karakas, A. I., et al. 2016a, A&A

Spina, L., Meléndez, J., & Ramírez, I. 2016b, A&A, 585, A152

Tucci Maia, M., Ramírez, I., Meléndez, J., et al. 2016, A&A, 590, A32

Valenti, J. A., & Piskunov, N. 1996, A&AS, 118, 595

Bedell et al.

TABLE 2
Line List and Measured Equivalent Widths.

Wavelength (Å)	Species	EP (eV)	log(gf)	Kepler-11 (mÅ)	HD1178 (mÅ)	HD10145 (mÅ)	HD16623 (mÅ)	HD20329 (mÅ)	HD21727 (mÅ)	HD21774 (mÅ)	HD28474 (mÅ)	HD176733 (mÅ)	HD191069 (mÅ)

Note. — Table 2 is published in its entirety in the electronic edition of ApJ. A portion is shown here for guidance regarding its form and content.

TABLE 3
DIFFERENTIAL ABUNDANCES [X/H].

Element	N_{lines}	Kepler-11	HD1178	HD10145	HD16623	HD20329	HD21727	HD21774	HD28474	HD176733	HD191069
CI	4	0.03 ± 0.01	0.12 ± 0.04	0.06 ± 0.12	-0.19 ± 0.08	0.05 ± 0.08	0.02 ± 0.06	0.18 ± 0.04	-0.07 ± 0.45	-0.00 ± 0.05	0.07 ± 0.03
OI	3	0.05 ± 0.01	0.18 ± 0.08	0.08 ± 0.02	-0.08 ± 0.02	0.18 ± 0.03	0.07 ± 0.03	0.20 ± 0.02	-0.25 ± 0.02	0.05 ± 0.03	0.14 ± 0.02
NaI	4	0.05 ± 0.02	-0.03 ± 0.02	-0.12 ± 0.05	-0.37 ± 0.02	-0.04 ± 0.04	-0.08 ± 0.03	0.27 ± 0.03	-0.54 ± 0.05	-0.03 ± 0.03	-0.01 ± 0.02
MgI	5	0.03 ± 0.05	0.39 ± 0.48	0.34 ± 0.48	-0.07 ± 0.55	0.12 ± 0.20	0.35 ± 0.47	0.36 ± 0.16	-0.27 ± 0.54	0.32 ± 0.48	0.35 ± 0.49
AlI	2	0.06 ± 0.01	0.18 ± 0.02	0.03 ± 0.00	-0.28 ± 0.01	0.18 ± 0.02	0.08 ± 0.00	0.28 ± 0.01	-0.45 ± 0.01	0.04 ± 0.00	0.11 ± 0.01
SiI	14	0.05 ± 0.02	0.04 ± 0.03	-0.00 ± 0.01	-0.27 ± 0.03	0.04 ± 0.05	0.02 ± 0.03	0.25 ± 0.02	-0.44 ± 0.04	-0.01 ± 0.02	0.04 ± 0.01
SI	4	0.04 ± 0.04	0.10 ± 0.04	0.05 ± 0.03	-0.23 ± 0.06	0.03 ± 0.09	0.01 ± 0.03	0.24 ± 0.03	-0.36 ± 0.09	0.02 ± 0.05	0.09 ± 0.05
KI	1	0.07 ± 0.00	0.07 ± 0.00	0.02 ± 0.00	-0.22 ± 0.00	0.03 ± 0.00	0.01 ± 0.00	0.15 ± 0.00	-0.42 ± 0.00	-0.00 ± 0.00	0.08 ± 0.00
CaI	11	0.06 ± 0.02	0.02 ± 0.14	-0.05 ± 0.17	-0.28 ± 0.05	0.18 ± 0.24	0.04 ± 0.15	0.19 ± 0.08	-0.47 ± 0.06	-0.07 ± 0.20	0.04 ± 0.03
ScI	4	0.09 ± 0.04	0.09 ± 0.03	0.02 ± 0.03	-0.30 ± 0.06	0.06 ± 0.06	0.03 ± 0.03	0.27 ± 0.03	-0.33 ± 0.08	-0.01 ± 0.04	0.08 ± 0.01
ScII	5	0.09 ± 0.02	0.14 ± 0.06	0.03 ± 0.02	-0.24 ± 0.04	0.14 ± 0.06	0.10 ± 0.05	0.32 ± 0.02	-0.41 ± 0.05	-0.00 ± 0.02	0.12 ± 0.04
TiI	18	0.07 ± 0.02	0.12 ± 0.03	0.05 ± 0.05	-0.21 ± 0.04	0.15 ± 0.03	0.07 ± 0.04	0.24 ± 0.04	-0.41 ± 0.03	0.02 ± 0.03	0.08 ± 0.02
TiII	11	0.07 ± 0.03	0.11 ± 0.05	0.01 ± 0.09	-0.18 ± 0.05	0.11 ± 0.03	0.01 ± 0.10	0.26 ± 0.04	-0.37 ± 0.04	-0.02 ± 0.03	0.11 ± 0.04
VI	9	0.08 ± 0.02	0.07 ± 0.02	-0.02 ± 0.03	-0.28 ± 0.03	0.08 ± 0.09	0.04 ± 0.03	0.28 ± 0.02	-0.48 ± 0.04	-0.00 ± 0.02	0.04 ± 0.02
CrI	10	0.04 ± 0.02	0.02 ± 0.03	0.01 ± 0.07	-0.47 ± 0.03	-0.06 ± 0.03	0.02 ± 0.03	0.27 ± 0.03	-0.60 ± 0.06	0.01 ± 0.03	-0.02 ± 0.02
CrII	5	0.05 ± 0.02	0.01 ± 0.02	-0.02 ± 0.05	-0.38 ± 0.06	-0.08 ± 0.02	0.01 ± 0.03	0.24 ± 0.03	-0.55 ± 0.05	-0.03 ± 0.04	-0.02 ± 0.02
MnI	8	0.06 ± 0.02	-0.04 ± 0.03	-0.07 ± 0.04	-0.61 ± 0.02	-0.18 ± 0.02	-0.04 ± 0.03	0.30 ± 0.03	-0.75 ± 0.06	-0.02 ± 0.03	-0.08 ± 0.02
FeI	92	0.06 ± 0.03	0.02 ± 0.04	-0.02 ± 0.06	-0.43 ± 0.09	-0.09 ± 0.05	0.01 ± 0.08	0.25 ± 0.08	-0.58 ± 0.08	-0.01 ± 0.05	-0.03 ± 0.09
FeII	17	0.06 ± 0.02	0.02 ± 0.05	-0.02 ± 0.11	-0.43 ± 0.07	-0.10 ± 0.05	0.00 ± 0.04	0.25 ± 0.03	-0.58 ± 0.07	-0.02 ± 0.03	-0.03 ± 0.04
CoI	6	0.07 ± 0.01	0.05 ± 0.04	-0.04 ± 0.03	-0.27 ± 0.04	0.01 ± 0.03	-0.01 ± 0.03	0.26 ± 0.01	-0.45 ± 0.03	-0.02 ± 0.01	0.06 ± 0.02
NiI	20	0.06 ± 0.02	0.00 ± 0.07	-0.03 ± 0.03	-0.42 ± 0.03	-0.05 ± 0.04	0.01 ± 0.05	0.31 ± 0.16	-0.60 ± 0.03	0.00 ± 0.05	-0.01 ± 0.02
CuI	4	0.08 ± 0.01	0.08 ± 0.03	-0.02 ± 0.02	-0.44 ± 0.05	0.00 ± 0.01	-0.00 ± 0.02	0.32 ± 0.03	-0.59 ± 0.09	0.06 ± 0.03	0.06 ± 0.02
ZnI	3	0.03 ± 0.04	0.05 ± 0.02	0.01 ± 0.04	-0.31 ± 0.06	0.07 ± 0.02	-0.00 ± 0.03	0.28 ± 0.05	-0.52 ± 0.09	0.00 ± 0.02	0.08 ± 0.02
YII	5	0.07 ± 0.02	-0.01 ± 0.01	-0.05 ± 0.03	-0.52 ± 0.03	-0.12 ± 0.03	-0.04 ± 0.02	0.23 ± 0.01	-0.61 ± 0.04	-0.04 ± 0.03	-0.08 ± 0.01
CH	3	0.03 ± 0.05	0.03 ± 0.12	-0.04 ± 0.13	-0.45 ± 0.11	-0.17 ± 0.09	-0.05 ± 0.09	0.24 ± 0.05	-0.65 ± 0.14	-0.08 ± 0.29	0.04 ± 0.08